# First results of the RPC commissioning at BESIII

Yuguang Xie [a,b,*], Jiawen Zhang [a], Jin Chen [a], Jifeng Han [a,b], Sen Qian [a,b], Hao Liang [c], Yongzhao Zhou [c], Yutie Liang [d]

[a] Institute of High Energy Physics, CAS, Beijing 100049, China
[b] Graduate University of Chinese Academy of Sciences, Beijing 100049, China
[c] University of Science and Technology of China, Hefei 230026, China
[d] Peking University, Beijing 100871, China

## ARTICLE INFO

## ABSTRACT

The commissioning of the RPC-based muon detector in the BESIII experiment has been carried out. The RPC modules, front-end electronics, online and offline software of the muon system have been studied. The detector performances including efficiency, counting rate, noise ratio, spacial resolution, dark current, and muon charge ratio were obtained by cosmic ray data with and without magnetic field. The new operating high voltage and threshold were chosen after the scan experiment. The long-term stability of the BESIII RPCs made of bakelite without oil treatment was studied.

© 2008 Elsevier B.V. All rights reserved.

## 1. Introduction

The Resistive Plate Chambers (RPCs) have been used widely in high energy physics and astroparticle physics experiments since theirs invention in 1981 [1]. RPC is a low cost gaseous detector with many advantages, such as large pulse, good time resolution and simple mechanical structure. In recent years, the main developments [2,3] of the RPC focus on the new resistive materials and surface treatments, new gap structures, new green and cheap gas mixtures, better time resolution within 60 ps, and higher rate capability beyond $kHz/cm^2$. The features of the RPCs currently running in some different experiments are summarized in Table 1.

It is well known that the biggest challenge of the RPC is its aging problem. Since the linseed oil treatment on the electrode surfaces has been proved as a crucial damage factor affecting the aging stability of RPC in BaBar [13–15], some experiments began to study new treatment methods with melamine or silicone, such as CMS, BESIII and INO [16]. The bakelite sheets for CMS are made in Italy with an improved technology and covered with a thin layer of melamine. The same effort has being made in China to improve the surface quality of the electrode since 2003. More than $1200\,m^2$, totally 978 RPC chambers have been manufactured for the BESIII muon system [17]. More details of the BESIII experiment can be found in Ref. [18]. The melamine treatment probably will be an important development of RPC material and technology in the future.

The BESIII muon counter (MUC) consists of nine layers of RPCs in the Barrel and eight layers in the Endcap, as shown in Fig. 1. In the X–Y plane, it is divided into eight segments in the Barrel and four segments in the Endcap. There are 72 RPC modules in the Barrel. Their dimensions vary from $1.05\,m \times 3.8\,m - 1.85\,m \times 3.8\,m$. While the 64 modules in the Endcap are octagon with area about $3.12 - 3.71\,m^2$. The cross-section of the module is illuminated in Fig. 2. Two layers of RPCs are designed to avoid the dead space and ensure the long-term performance. There are three, four or five RPCs in each layer of a module. The height of each module is about 32 mm.

The readout strips are arranged according to Fig. 1. The strips in the Endcap are all 35 mm wide and 0.92–2.11 m long. Each Endcap module has one set of 64 strips in X or Y direction. The strips in the Barrel are 20–39 mm wide from the inner to the outer layer. The 48 strips of each module in the odd layer are in Z direction and 3.72 m long. While the 96 strips of each module in the even layer are in $\phi$ direction and 0.28–1.66 m long. For those modules in the even layers of the top segment, 16 strips at the east end are cut into two by the liquid helium access. The RPC signals are collected and read out by the front-end chips (FECs). Each FEC can read out 16 contiguous strips, and maximum 16 FECs compose a data chain. Total of 9152 channels are read out by 572 FECs of 40 data chains.
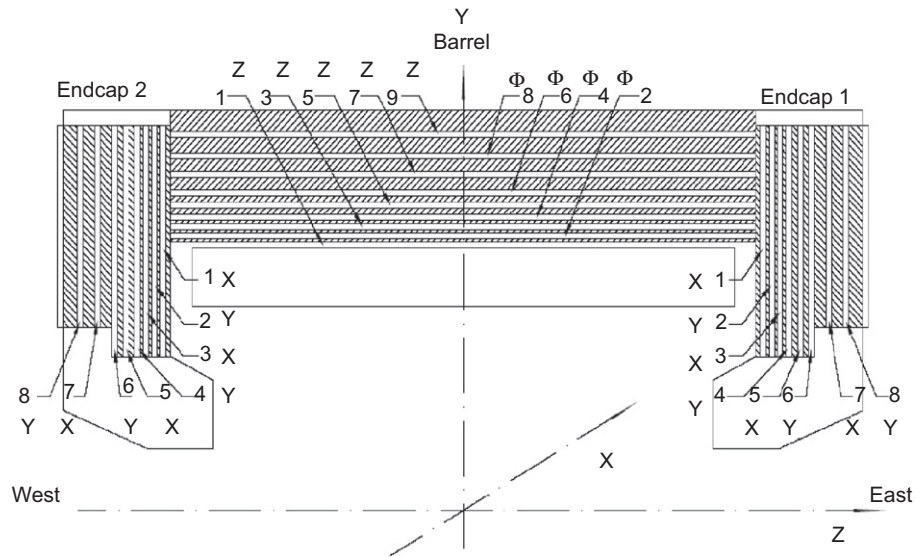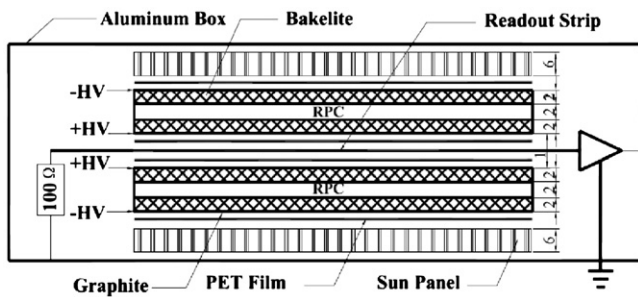
* Corresponding author at: Institute of High Energy Physics, CAS, Beijing 100049, China. Tel.: +86 108823 6412; fax: +86 108823 3083.
E-mail address: ygxie@mail.ihep.ac.cn (Y. Xie).
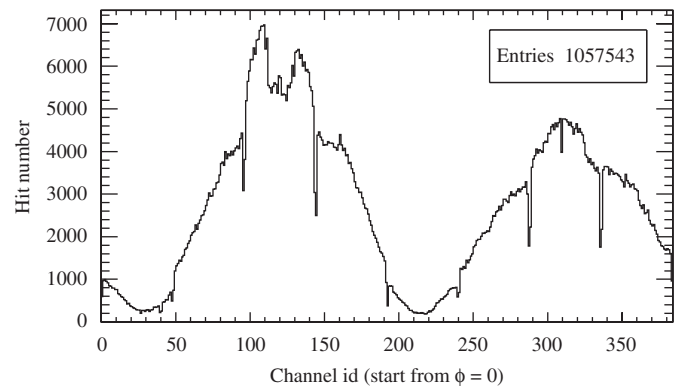
**Table 1**
Main features of RPCs now running.

| Experiment | Function | Mode | Material | Treatment | Gaps | Readout |
|---|---|---|---|---|---|---|
| ATLAS [4] | trg | ava | Bak | Oil | 1 | $X$ and $Y$ (30–40 mm) |
| CMS [5] | trg | ava | Bak | Melamine/oil | 2 | $X/Y$ (20–40 mm) |
| STAR [6] | tof | ava | Glass | – | 6 | Pads |
| ALICE [7,8] | trg/tof | str/ava | Bak/glass | Oil/– | 1/10 | $X$ and $Y$/pads |
| BaBar [9] | mu ID | str | Bak | Oil | 1 | $X$ and $Y$ |
| Belle [10] | trg | str | Glass | Oil | 2 | strip |
| YBJ-ARGO [11] | EAS imaging | str | Bak | – | 1 | Pads ($56 \times 62\,cm^2$) |
| BESIII [12] | mu ID | str | Bak | Melamine | 2 | $X/Y$ (20–40 mm) |



**Fig. 1.** Layout of BESIII muon counter.



**Fig. 2.** The cross-section of RPC module.



**Fig. 3.** The hitmap of layer 6 in the Barrel. The ordering starts from $\phi = 0$ in counter-clockwise and includes eight segments (48 $Z$ strips in each segment).

The gas mixture of argon:F134a:*iso*-butane (50:42:8) is used and controlled by the MKS 2179*A*&247*D* system. The output flow of the mixing tank is about 2083 CC/min and split into 136 channels. The gas ratio is monitored real time by three ionization chambers [19]. The high voltage system contains 46 pairs of positive and negative channels. Each pair of channels are split to supply three modules and controlled by the BESIII slow control system [20].

## 2. Online DAQ and offline software

The commissioning data is acquired by the online DAQ system and analyzed by the offline software. The online DAQ hardware for

MUC consists of one VME crate and 10 readout modules. Two trigger conditions are often used for the tests: the Barrel TOF back to back (BTOF_BB) and the number of hits in the Barrel TOF$\geqslant 2$ (NBTOF2). The trigger rate is about 75 and 280 Hz, respectively. By the hitmap of online display, some dead channels and two hot channels were found and fixed. The typical hitmap of the MUC after BTOF_BB triggering is shown in Fig. 3.
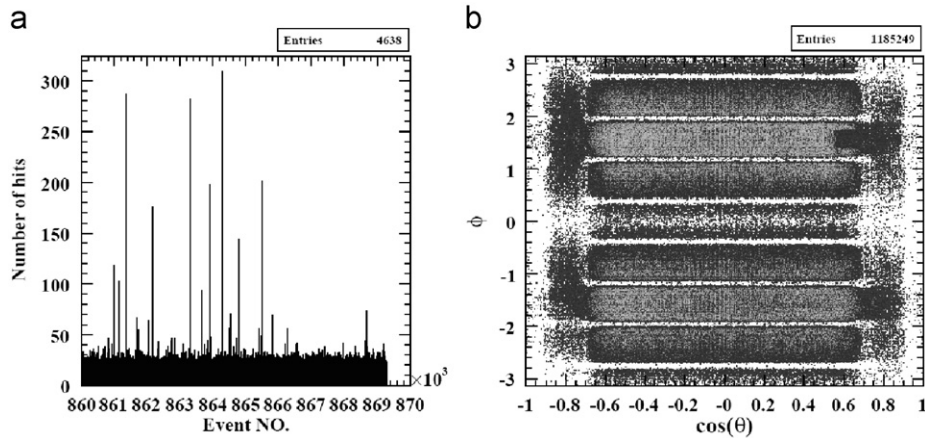
**Fig. 4.** Offline histogram examples. (a) Hit number versus event. (b) The plots of $\phi$ and $\cos(\theta)$ of the muon track positions at the innermost layer. The clear MUC structure can be seen, including the Endcap and the Barrel, segments of the Barrel, and the liquid helium access.
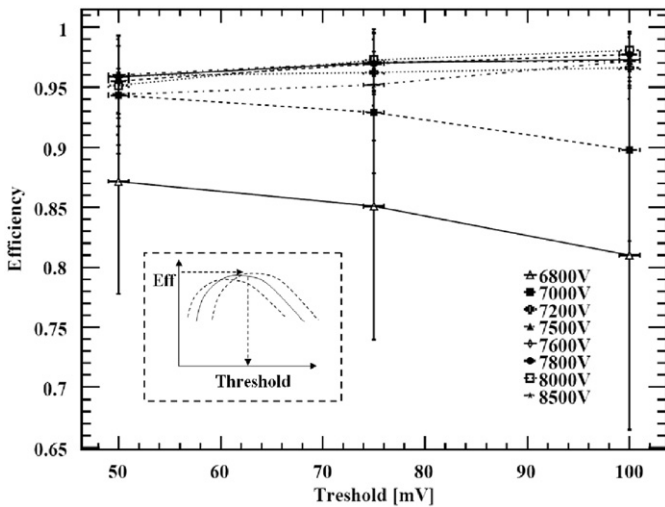


**Fig. 5.** The average efficiency of modules in the Barrel versus the threshold at different high voltage points. The dashed-line box shows the full expected curves at three different high voltage scales.



**Fig. 6.** The resolution of the Barrel versus the threshold at different high voltage points. The dashed-line box shows the full expected curves at three different high voltage scales.
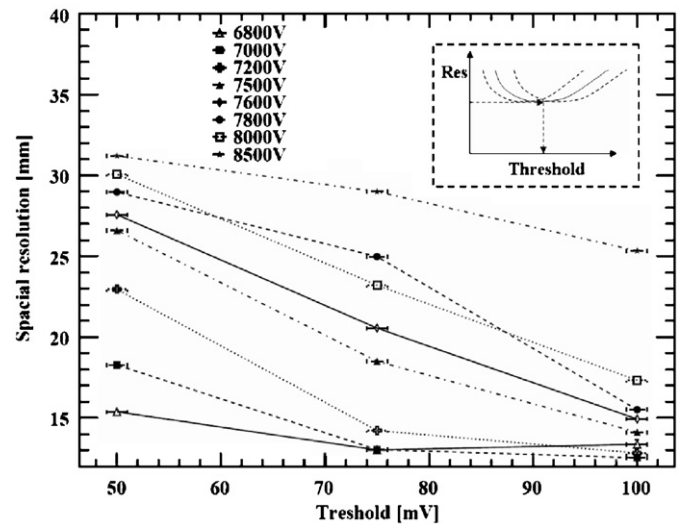
More detailed results, including detection efficiency, counting rate, noise ratio, spacial resolution, cluster size distribution, can be obtained by the MUC offline software. Two simple examples are shown in Fig. 4(a) and (b). The former shows the hit number of cosmic ray event. The average hit number is about 14 hits. The maximum hits could be more than 300 due to the big air showers. The latter illustrates the hit positions of muon tracks at the innermost layer after reconstruction. Both examples can be used for the data quality monitor (DQM) of the muon detector.

## 3. Scan experiment

For the streamer mode RPC, the high voltage and the discrimination threshold are two important operating parameters to be optimized. Generally speaking, the lower high voltage is more favored, and the proper threshold is also required relatively lower to guarantee the performance. Usually, $\pm 4$ kV is used as the

high voltage and 100 mV as the threshold. However, the parameters could be adjusted for better operation in different environments. So the scan experiment was carried out in the commissioning. Three threshold points, 100, 75, 50 mV, and totally 28 high voltage points were tested. At each threshold, the high voltage was set from 6.8 to 9 or 8.5 kV by 200 or 250 V steps. During the experiment, the temperature varied within $21 \pm 1\,^\circ$C and the humidity was within $40 \pm 8\%$. The gas mixture ratio was also fixed.

### 3.1. Threshold selection

In principle, the selected threshold should maximize the Signal Noise Ratio. For BESIII RPC, it is reflected in the efficiency, resolution, average hit number and noise ratio. With regard to the efficiency, low threshold does introduce more noise and depress the efficiency, while high threshold will lose some efficiency, just like the dashed-line box in Fig. 5 shows. For the resolution, the
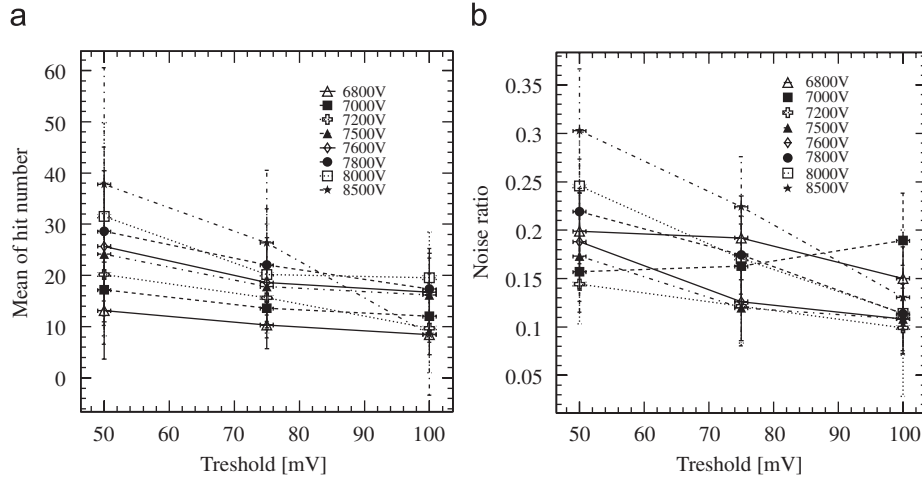
a

b



**Fig. 7.** The hit number (a) and noise ratio (b) versus the threshold at different high voltage points.
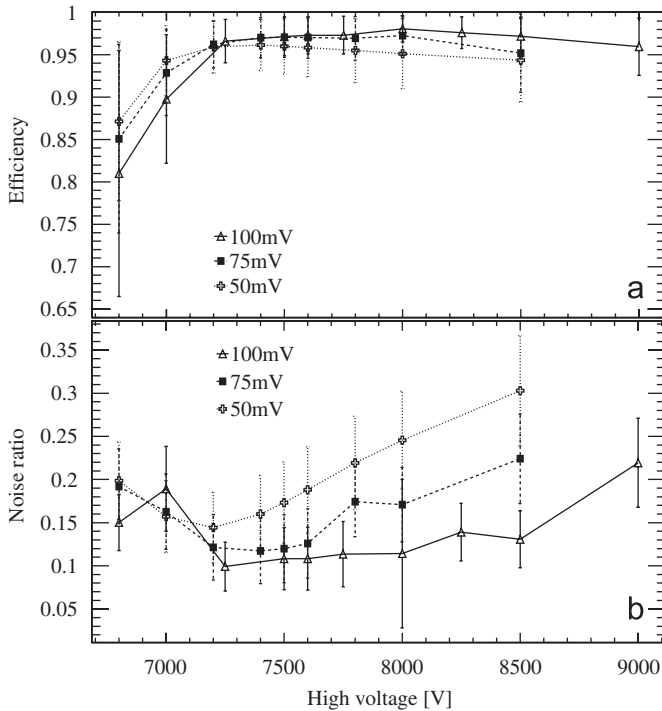


**Fig. 8.** The average efficiency of modules in the Barrel (a) and noise ratio (b) versus the high voltage at different thresholds.

similar conclusion can be drawn. More noise makes the resolution worse, and low efficiency loses more hits and then also makes the resolution worse, as the dashed-line box in Fig. 6 shows. So the proper threshold is to make both the efficiency and resolution highest. Since the thresholds tested here are not higher than 100 mV, the full curves of efficiency versus threshold and resolution versus threshold cannot be seen in the test results. However, the results are consistent with the expected in the low threshold range, i.e Figs. 5 and 6.

In Fig. 7, both hit number and noise ratio decrease along with threshold increasing as expected. Here the noise ratio is defined as the number of hits not used by reconstruction over the total hits in an event. The result shows that higher threshold is preferred. By

preliminary consideration, the 100 mV threshold is the best, and the 75 mV threshold is acceptable. But the 50 mV threshold is too low to be used.

### 3.2. High voltage selection

The efficiency plateau curve is the main basis of high voltage selection for the streamer mode RPC. The high voltage chosen should be in the plateau. As shown in Fig. 8(a), the plateau-start high voltage is near 7.2 kV for all the three thresholds, and the efficiency plateaus extend to 8.5 kV, even 9 kV. So a large range is available. Furthermore, the noise ratio is also sensitive to the high voltage. As seen in Fig. 8(b), the optimal high voltage is $7.4 \pm 0.2$ kV. If the high voltage goes lower, the efficiency will be lost, and the noise ratio rises. Contrarily, more noise will be introduced.

Considering the spacial resolution, the favorable high voltage can be found at the trough of the curve. As shown in Fig. 9(a), it is close to 7 kV. Seen from Fig. 9(b), the low high voltage is more reasonable for the hit number. So the relative lower high voltage is better.

### 3.3. Combined selection

As discussed above, the threshold and high voltage should be selected by comprehensive consideration according to the efficiency, noise ratio, resolution, and hit number. The scan results are summarized in Table 2, in which the mark "–" means rejected while "$\sqrt{}$" indicates acceptable. Since we want to find a lower high voltage for RPC operating, only those points $\leqslant 8$ kV are included. Obviously, the lowest workable high voltage is about 7.2 kV with threshold 75 or 100 mV. Actually, each high voltage channel supplies three RPC modules and the threshold of each data chain can be adjusted independently. So the fine adjustment by group is more reasonable for both high voltage and threshold. Finally, $7.2 \pm 0.2$ kV and 75 mV are used for both Barrel and Endcap modules.

### 4. RPC performance

After the scan experiment, the detection efficiency is concerned firstly. It can be checked at three levels: layer, module
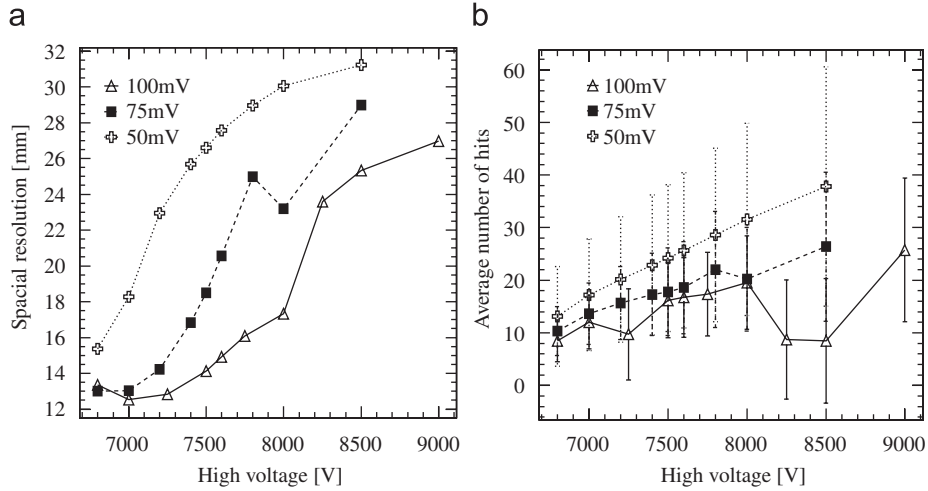
**Fig. 9.** The resolution of the Barrel (a) and hit number (b) versus the high voltage at different thresholds.

**Table 2**
Threshold and high voltage scan result.

| Thrs (mV) | Crt | 7.2 kV | 7.4 kV | 7.5 kV | 7.6 kV | 7.8 kV | 8 kV |
|-----------|-----|--------|--------|--------|--------|--------|------|
| 100 | Eff | ✓ | ✓ | ✓ | ✓ | ✓ | ✓ |
| | Nos | ✓ | ✓ | ✓ | ✓ | ✓ | ✓ |
| | Res | ✓ | ✓ | ✓ | ✓ | ✓ | ✓ |
| | Hit | ✓ | ✓ | ✓ | ✓ | ✓ | ✓ |
| 75 | Eff | ✓ | ✓ | ✓ | ✓ | ✓ | ✓ |
| | Nos | ✓ | ✓ | ✓ | ✓ | – | – |
| | Res | ✓ | ✓ | ✓ | ✓ | – | – |
| | Hit | ✓ | ✓ | ✓ | ✓ | – | – |

and strip. The distributions of efficiency at each level are shown in Fig. 10(a)–(c). The averages are 96.4%, 94% and 94.3%, respectively.

Concerning the background, it can be seen from the noise ratio, single counting rate, and dark current. Given the definition in Section 3.1, the average noise ratio of 0.19 implies that averagely two or three hits give no contribution to the track reconstruction in an event. By using the random trigger of 1 kHz with 800 ns window, the single counting rate was measured with average result of 0.023 Hz/cm$^2$. As for the counting rate of cosmic ray after back to back triggering, is only about $4 \times 10^{-4}$ Hz/cm$^2$. In addition, the dark currents of all positive and negative high voltage channels were also recorded by the slow control system and saved to the database. The analyzed result shows that the dark currents are at a very low level, only 0.5 μA/m$^2$. Conclusively, the noise background of all RPC modules is low, as shown in Fig. 11.

The spacial resolution and the cluster size are also important. The spacial resolution is basically determined by the strip width, i.e, $\sigma = w/\sqrt{12}$. In addition, it is also affected by the reconstruction method and track incident angle. In Fig. 12(a), the resolutions in the Barrel from layer 2 to 6 are 16 to 22 mm as expected. Moreover, the effect caused by the reconstruction and incidental angle is obvious in both the inner and the outer layers. In these layers, the resolutions become worse but less than 50 mm. It is difficult to avoid this effect. A cluster in MUC is defined as the continuous

fired strips. Normally, the average cluster size is less than 2, as shown in Fig. 12(b). The clusters with size >4 are rare, which ratio is at 1‰ scale and mainly due to the cosmic ray air shower.

## 5. Cosmic ray with magnetic field

By using the magnetic field offered by the superconducting magnet, the obvious bending effect of the cosmic rays can be seen in Fig. 13(a). The muon charge ratio, i.e $\mu^+/\mu^-$, also can be calculated. The bending will change the $\phi$ angle in $X$–$Y$ plane of a muon track momentum. We define $\Delta\phi$ as the difference of the $\phi$ angles of two track segment momentums, i.e $\Delta\phi = \phi_+ - (\phi_- + \pi)$. So, for $\mu^+$, $\Delta\phi < 0$, for $\mu^-$, $\Delta\phi > 0$. As shown in Fig. 13(b), the $\Delta\phi$ distribution is not symmetrical and cannot be fitted well by Gaussian function. The calculation uses only the MUC information, and the events pass the following selections: (a) *NTrack* = 2, (b) *HitsOfEachTrack* ⩾ 4, (c) $\phi_1 \times \phi_2 < 0$. The result gives $\mu^+/\mu^- = 1.2368 \pm 0.0032$ (statistical) that is consistent with the PDG value: 1.1–1.4 [21].

## 6. Long-term study

So far, the BESIII RPCs have been tested many times since 2005. The test history is listed in Table 3. The efficiency test results have been accumulated more than three years. These data are the important sources for RPC long-term study.

All the test results are filled into Fig. 14(b), in which the average efficiency is 93.8%. The average efficiency of modules tested at each time is drawn with the open triangle up in Fig. 14(a). In fact, not all 136 modules were tested at each time, and the test conditions and systems may be different. We can see that the average efficiency is not very high. It is due to some modules with relative low efficiency especially those in the Endcap. In fact the Endcap modules were firstly produced in our new product line. The gluing technics was not ripe yet and resulted in chamber plumping and gas leakage. This quality problem appeared in about 11 modules. However, as the open cross shown, many modules have excellent efficiency, even up to 98%. After some maintenance during the commissioning,
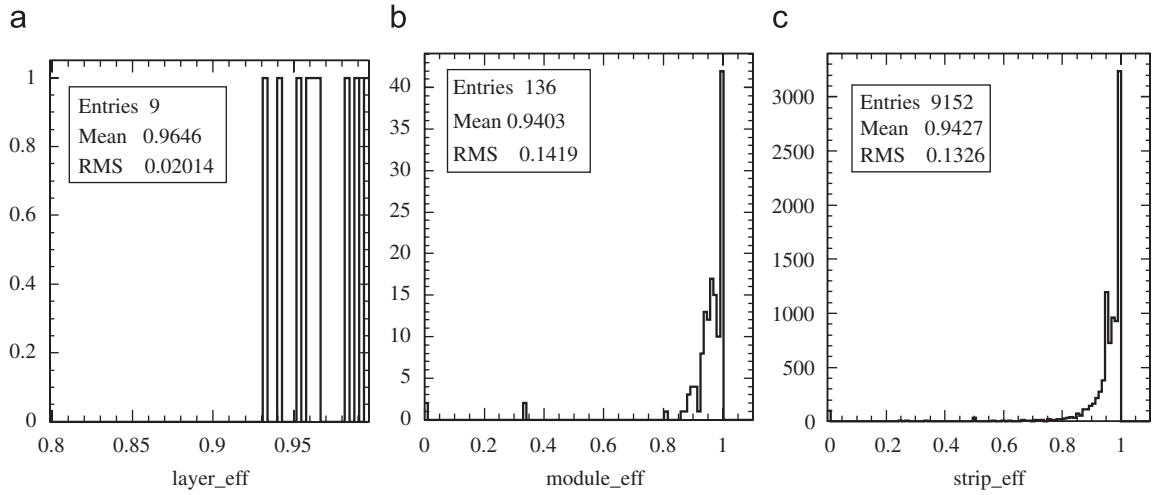
**Fig. 10.** RPC efficiency at layer (a), module (b) and strip (c) levels. Layer 0–7 include both Endcap and Barrel modules, while layer 8 includes only Barrel modules.
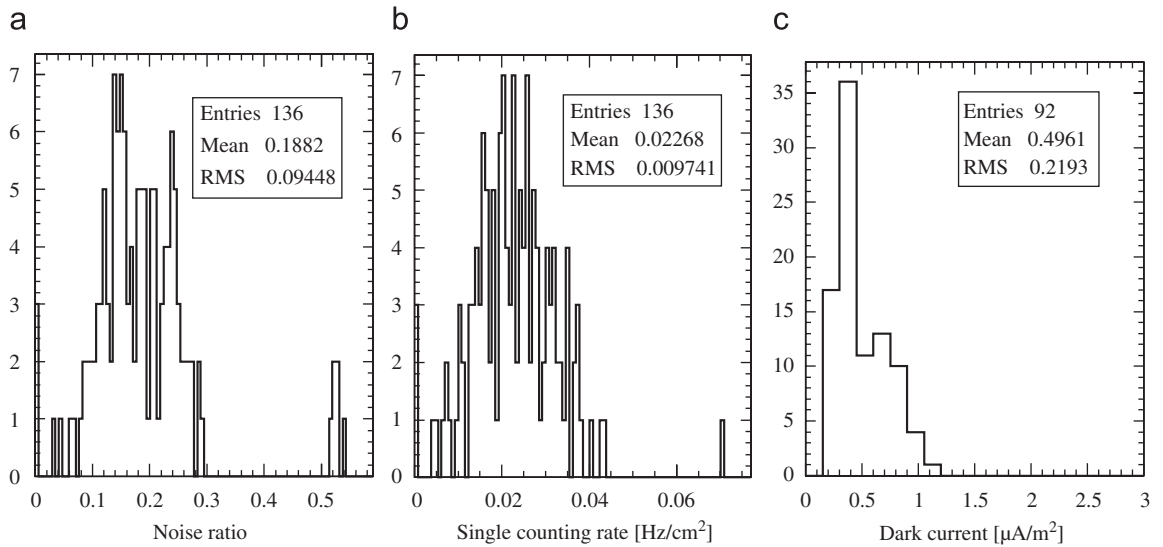


**Fig. 11.** RPC noise background at module level: (a) noise ratio, (b) single counting rate, (c) dark current.
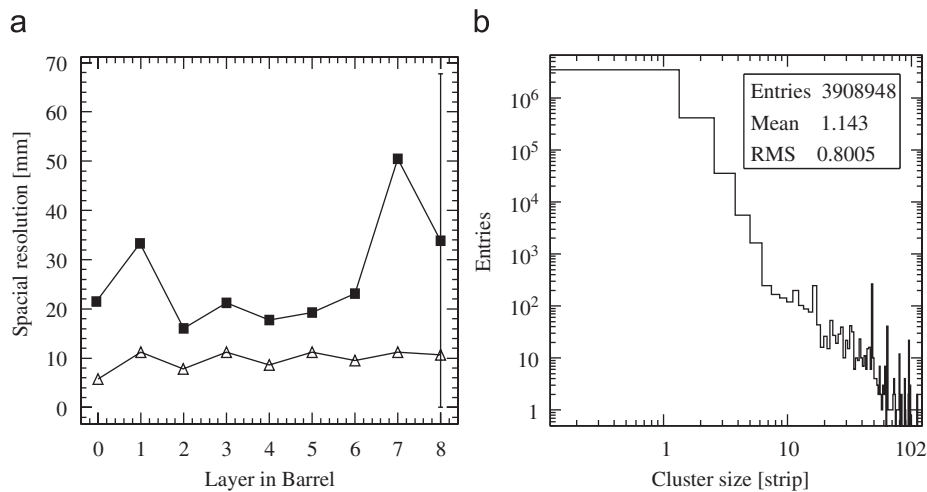


**Fig. 12.** (a) MUC spacial resolution of the Barrel, the blank markers show the intrinsic, and the solid markers show the resolution of reconstruction. (b) Cluster size distribution.
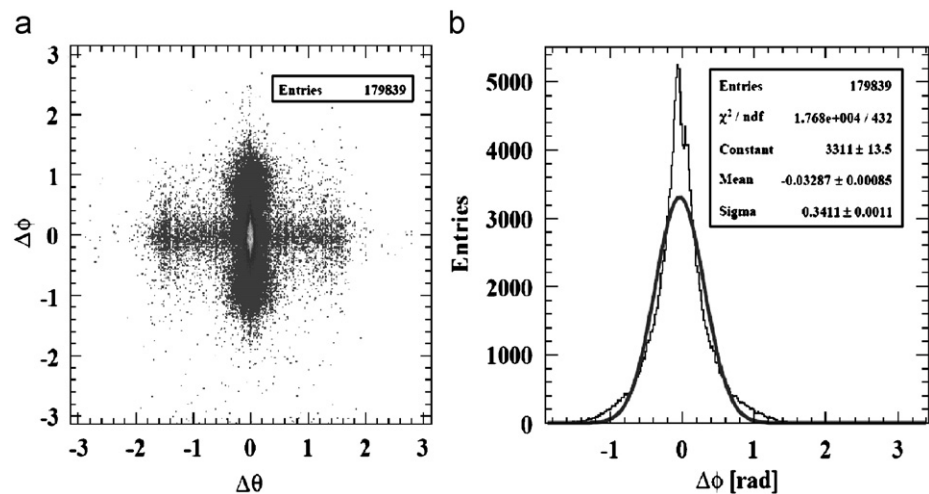
**Fig. 13.** (a) The plots of $\Delta\phi$ and $\Delta\theta$ of two muon track momentum after event selections, from cosmic ray data in magnetic field (0.9T, −Z). (b) The $\Delta\phi$ distribution projected from (a).

**Table 3**
Test history of the BESIII RPC modules.

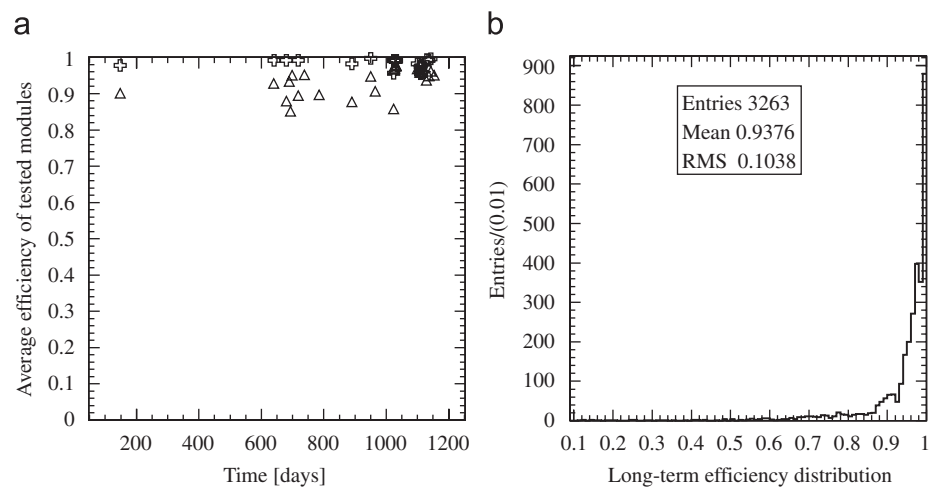| Time | Goal | Test system |
| --- | --- | --- |
| May–October, 2005 | QC | NIM&SelfTest |
| February–December, 2007 | Monitor | NIM&SelfTest |
| June–July, 2008 | Commissioning | DAQ&offline |



**Fig. 14.** The long-term efficiency of RPC modules. (a) The average efficiency versus time, the open triangle up denotes the average of all module tested at a time, and the open cross denotes the efficiency of a good module. (b) The distribution of all efficiency test results.

the average efficiency of all modules is about 94%, as shown in Fig. 10(b).

## 7. Summary and conclusions

In the commissioning of the RPC muon counter, many hardware problems were encountered and solved, both online and offline software were checked and proved the validation. Now the muon counter is in good status for the coming data challenge, and its current performance is still very good after adjusting the high voltage and threshold. The long-term efficiency shows that the new bakelite material and surface treatment has a good development future.

## References

[1] R. Santonico, R. Cardarelli, Nucl. Instr. and Meth. A 187 (1981) 377.
[2] P. Fonte, IEEE Trans. Nucl. Sci. NS-49 (2002) 3.
[3] G. Bruno, Eur. Phys. J. C 33 (2004) s01, s1032Cs1034.
[4] ATLAS Collaboration, Muon Spectrometer Technical Design Report, CERN/ LHCC/97-22 (2002).
[5] CMS Collaboration, CMS Muon Technical Design Report, CERN/LHCC/97-32 (1997).
[6] W.J. Llope, et al., Nucl. Instr. and Meth. B 241 (2005) 306.
[7] R. Arnaldi, et al., Nucl. Phys. B (Proc. Suppl.) 158 (2006) 21.
[8] M. Spegel, et al., Nucl. Instr. and Meth. A 453 (2000) 308.
[9] B. Aubert, et al., Nucl. Instr. and Meth. A 479 (2002) 1.
[10] A. Abashian, et al., Nucl. Instr. and Meth. A 479 (2002) 117.
[11] G. Aielli, et al., Nucl. Instr. and Meth. A 562 (2006) 92.
[12] J.W. Zhang, et al., Nucl. Instr. and Meth. A 540 (2005) 102.
[13] F. Anulli, et al., Nucl. Instr. and Meth. A 539 (2005) 155.
[14] F. Anulli, et al., Nucl. Instr. and Meth. A 552 (2005) 276.
[15] H.R. Band, et al., Nucl. Instr. and Meth. A 594 (2008) 33.
[16] S. Biswas, et.al., arXiv:0802.2766v1 [nucl-ex], 20 February 2008.
[17] J.W. Zhang, et al., Nucl. Instr. and Meth. A 580 (2007) 1250.
[18] F.A. Harris, et al., Nucl. Phys. B (Proc. Suppl.) 162 (2006) 345.
[19] S. Qian, et al., Nucl. Instr. and Meth. A 595 (2008) 520.
[20] X.H. Chen, et al., Nucl. Instr. and Meth. A 592 (2008) 428.
[21] C. Amsler, et al., Phys. Lett. B 667 (2008) 1.